

Single silicon waveguide MRR based Fano resonance in the whole spectral bands*

LU Lidan¹, WANG Shuai¹, ZENG Zhoumo², DONG Mingli¹, and ZHU Lianqing^{1**}

1. School of Instrument Science and Opto Electronics Engineering, Beijing Information Science and Technology University, Beijing 100016, China

2. Department of Precision Instrument Engineering, Tianjin University, Tianjin 300072, China

(Received 18 September 2021; Revised 12 April 2022)

©Tianjin University of Technology 2022

To improve the integration of Fano devices, we design a T-shaped waveguide coupling micro-ring resonator (MRR) structure to achieve a single cavity with Fano resonance in the whole spectral bands. The mathematical relationship between the phase factor, the coupling coefficient of the bus waveguide, and the Fano resonance slope extinction ratio (ER) is established. The electron beam exposure process is used to obtain a device with an insertion loss of ~ 3 dB. The maximum ER of the Fano lineshape exceeds 15 dB, and the slope ratio (SR) is 251.3 dB/nm. This design improves the compactness of the Fano resonant device.

Document code: A **Article ID:** 1673-1905(2022)07-0398-6

DOI <https://doi.org/10.1007/s11801-022-1150-6>

Fano resonance is a phenomenon that can enhance the slope of spectrum resonating between a cavity in a discrete state and a cavity in a continuous state^[1,2]. Until now, silicon waveguide-based Fano resonance has been used to develop sensors^[3-5], modulators^[6,7], and switches^[8-10], which require high integration and low loss. Thus, it is desirable to reduce the size of the device further. The high integration reduces the system's overall size, thereby reducing power consumption and transmission loss. The Fano resonance on a silicon photonic platform depends on the coupling of two microcavities. Therefore, a high-Q factor resonant cavity coupled with the bus waveguide to form a Fano resonance needs to be developed to improve compactness.

Most of the Fano resonance devices on silicon photonics are derived from the quasi-continuous and discrete modes coupling. Under certain conditions, the Fano resonance lineshape, electromagnetic induced transparency, or Lorentzian lineshape are co-existent in the adjacent resonance mode. If intensity demodulation is used, lasers and detectors with specific wavelengths must be selected, not conducive to practical applications.

Only three cases reported that all resonance modes were Fano linear. LU et al^[11] reported a structure composed of two coupled micro-ring resonators (MRRs) with the same radius. Two MRRs have a quasi-continuous spectrum mode and a discrete mode, respectively. Although each resonance mode of the transmission spec-

trum is Fano lineshape, the device sacrifices the compactness of the MRR. GU et al^[12] inserted an air hole into the bus waveguide to obtain a continuous state with a positive phase delay and coupled it with the discrete state MRR. All resonance peaks were Fano resonance line-shaped, and the slopes were all positive. The loss and Fano lineshape can be adjusted according to the size and position of the air hole. Our groups^[13] developed a new structure composed of a T-shaped bus waveguide coupled MRR in simulation without experiment verification. The spectrum is all Fano resonance lineshape, and the slopes are all negative. However, the slope of the spectrum enhances with a small increment.

Here, to realize the Fano resonant device with a compact structure and an antisymmetric lineshape at all resonance peaks in the experiment, we introduce a T-shaped waveguide structure in the bus waveguide of the single MRR device. The generated Fano lineshapes have large tolerances of the structure designs and fabrications. Moreover, we expect the T-shaped-enabled Fano resonance lineshapes in the waveguide-MRR could be employed to improve the performance by employing two T-shaped waveguides.

In Fig.1, we built the device on a silicon on insulator (SOI). The standard thickness of the SOI's top layer silicon is 220 nm, and the buried layer silicon dioxide is 2 μm . The device consists of MRR and a T-shaped waveguide. T and d are the length of the T-shaped

* This work has been supported by the State Grid Zhejiang Electric Power Corporation Information Telecommunication Branch (No.B311XT21004G), the 111 Project of China (No.D17021), the National Natural Science Foundation of China (No.61903042), and the Beijing Natural Science Foundation (No.4214081).

** E-mail: zhulianqing2020@126.com

waveguide and the coupling gap between the microring and bus waveguide, respectively. The T-shaped waveguide's width is the same as the width of the MRR. When the broadband communication band light is incident on the device, a part of it is transmitted in the bus waveguide, and the rest of the incident light enters the microring to form a discrete resonant wave. For the existence of a T-shaped waveguide, the incident light is transmitted in the bus waveguide with the amplitude of $tE_{in}e^{-i\Delta\phi}$, where t is the transmission coefficient of the coupling region. The other part of the light with the amplitude of $i\kappa E_{in}$ is coupled into the MRR, where $i\kappa$ is the coupling coefficient. The light with the amplitude $E_1=i\kappa\alpha e^{i\delta}E_{in}$ will be coupled back to the bus waveguide again in the MRR, where $\delta=2\pi nR/\lambda$ is the phase delay of one cycle in MRR, and α is the amplitude transmission coefficient of one revolution in MRR. n is the effective refractive index of the propagation mode, λ is the operating wavelength, and L is the perimeter of the MRR. When E_1 passes through the waveguide-MRR coupling region, the part with the amplitude of tE_1 propagates continuously in the MRR, and the other part with the amplitude of $i\kappa E_1$ couples to the bus waveguide, which will be on the output port of the bus waveguide. The light would pass through many cycles. Thus, the light intensity of the output for through port is

$$T(\lambda) = |E_o / E_i| = \frac{\left| \frac{\overbrace{tE_0 \cdot e^{-i\Delta\phi}}^{\text{continuous}} + \overbrace{i\kappa E_1 + i\kappa E_2 + \dots}^{\text{discrete}}}{E_i} \right|^2}{\left| \frac{tE_1 e^{-i\Delta\phi} + i\kappa(i\kappa)\alpha e^{i\delta} E_1 + i\kappa(i\kappa)t\alpha e^{i2\delta} E_1 + \dots}{E_i} \right|^2} = \left| \frac{te^{-i\Delta\phi} - \frac{\kappa_1 \kappa_2 \alpha e^{i2\pi^2 nR/\lambda}}{1 - t\alpha e^{i2\pi nL/\lambda}}}{E_i} \right|^2 \quad (1)$$

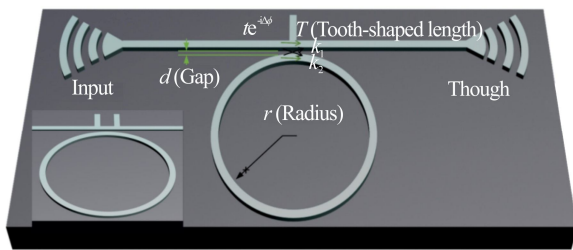
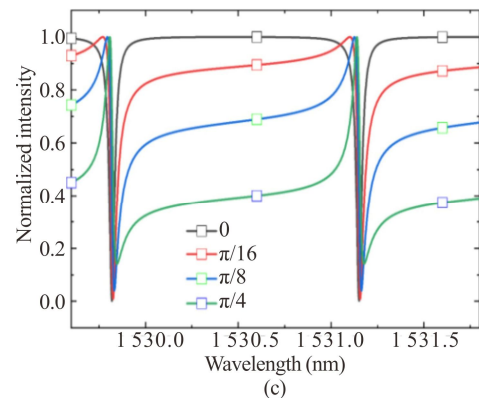
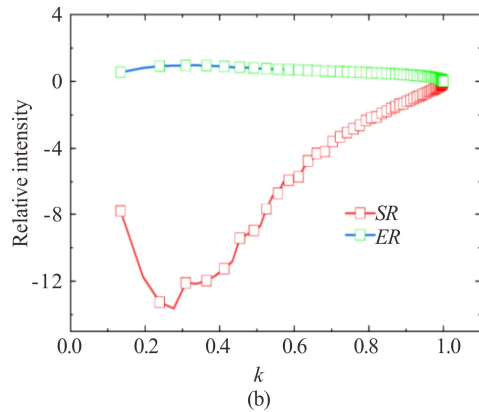
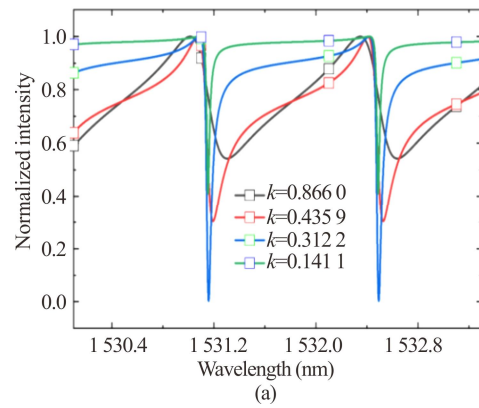


Fig.1 Structure of T-shaped waveguide coupled MRR

To obtain the detailed parameters of the influence of the phase delay $\Delta\phi$ and the coupling coefficient on the resonance lineshape, we simulate the transmission spectrum by setting $\kappa=0.312$, $R=30\ \mu\text{m}$ and $\alpha=0.95$. The normalized transmission spectra obtained according to Eq.(1) are shown in Fig.2(a) and (b). The extinction ratio

(ER) and slope ratio ($|SR|$) of the Fano resonance spectra are greater when $\kappa=0.29$. The negative sign of SR indicates that the slope direction is negative. When $\kappa>0.29$, the increase of κ leads to a decrease in $|SR|$, which is consistent with the results reported by our group^[13]. The phenomenon can be achieved experimentally by reducing the gap between the bus waveguide and the microring. As shown in Fig.2(c) and (d), it can be seen that when the phase factor $\Delta\phi$ is 0, the transmission spectrum is a symmetrical Lorentzian lineshape. When different phase factors are introduced, the transmission spectrum appears symmetric differently. The SR reaches its best at $\Delta\phi=0.4798$. All resonance peaks are asymmetrical lineshape. Thus, we can obtain Fano asymmetrical lines with different characteristics by adjusting the coupling coefficient and phase factor parameters.



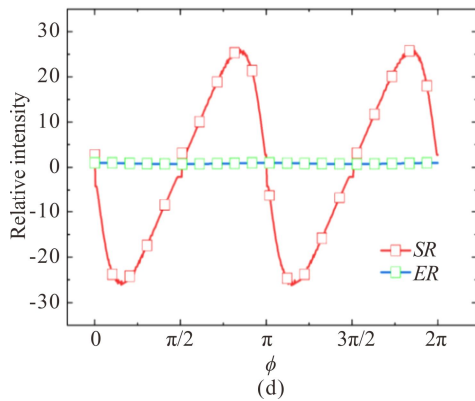


Fig.2 Curves of single cavity Fano resonance: (a) Normalized transmission spectra under different coupling coefficients; (b) SR and ER at the Fano resonance wavelength of 1 531.2 nm under different coupling coefficients; (c) Normalized transmission spectra under different phase factors; (d) SR and ER at the Fano resonance wavelength of 1 531.2 nm under different phase factors

The three-dimensional finite difference time domain (3D-FDTD, Lumerical Solutions Inc.) method is used to obtain and optimize the device's transmission spectrum, and the device's structural parameters are set to radius $R=30\ \mu\text{m}$, T-shaped waveguide length $T=1\ \mu\text{m}$, and wavelength's width is 450 nm. The wavelength range is 1 500—1 600 nm. The Fano resonance spectrum is obtained in Fig.3. The obtained SR and ER are 265 dB/nm and 35 dB, respectively, and figure of merit $FOM=9\ 275$, which is higher than similar devices reported in Refs.[11,12].

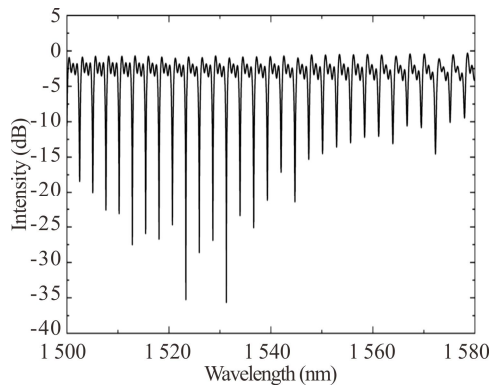


Fig.3 Transmission spectrum at $R=30\ \mu\text{m}$

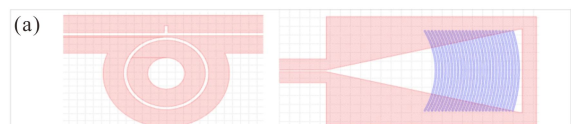
The device is fabricated on an SOI chip with a 220-nm-thick top silicon layer, 2- μm -thick buried silicon dioxide and 700- μm -thick substrate silicon. The device is patterned with electron beam lithography and inductively coupled plasma etching. The input light source and output detection are realized through the vertical coupling grating. An 8-inch SOI is diced with the feature size of 1.5 cm \times 1.5 cm. The dicing channel width is 180 μm . We used a cotton ball with acetone liquid to scrub the SOI.

Acetone, isopropanol, and deionized water in an ultrasonic machine for 10 min are followed. As shown in Fig.4(b), the processing is as follows.

Spin coater centrifuges the positive electron beam photoresist (Type: ZEP520A-7) on SOI at 3 000 rpm for 1 min. It takes about 5 min to bake at a temperature of 150 $^{\circ}\text{C}$. Electron beam lithography (Type: Vistec EBPB 5000plus) with an exposure dose of 190 $\mu\text{c}/\text{cm}^2$ is used to the pattern. The ZED-50 developer is used for pattern development. The SF_6 and O_2 are used as the inductively coupled plasma etching (Type: Oxford plasma lab system 100). The grating coupler etches for 10 s and a groove with a height of 150 nm is formed, and the rest waveguide is etched for 32 s with a 220 nm height. The organic solvent (Type: N, N-dimethylformamide) is soaked for 30 min to remove the remaining resist.

Micrographs taken from a scanning electron microscope (SEM) of a silicon photonic device are shown in Fig.5. From the cross-section (Fig.5(a)) and top view (Fig.5(b)) of vertical coupling grating, it can see that the etching edge is vertical with a certain roughness. Fig.5(d) and (e) are the enlarged SEM images of the T-shaped waveguide and MRR's coupling region. The width of the waveguide and the MRR strip waveguide are the same (440 nm). The coupling gap is 142 nm, and the MRR radius is 30 μm . The length of the side-coupled single T-waveguide is 1 μm , and the distance from the middle of the coupling region is also 1 μm . A light source with a broadband spectral wavelength of 1 530—1 610 nm is coupled to the bus waveguide through a vertical grating coupler. The light source is aligned with the semi-automatic coupling platform, as shown in Fig.6, using an optical fiber, and the signal output is also connected to the optical spectrometer in the same way (Type: AQ6370D, resolution: 0.02 nm).

The device loss mainly comes from several aspects. Rectangular waveguide side scattering is usually 2—3 dB/cm, and the general roughness measured by the atomic force microscope is 2.8 nm/rms. According to the roughness, the scattering loss of the waveguide sidewall can be simulated. The loss caused by the process error mostly comes from the scattering caused by the roughness of the waveguide sidewall. The silicon material loss of passive devices is negligible, but the silicon material loss caused by doping is relatively large. For example, the material absorption loss of the electro-optic modulator based on the plasma effect is greater than the material absorption loss caused by thermal modulation. The mode mismatch loss comes from the scattering of the sharply curved waveguide. Currently, when curved waveguides have a radius of not less than 5 μm , the loss can be neglected. Therefore, the transmission loss mainly comes from edge scattering loss in this case.



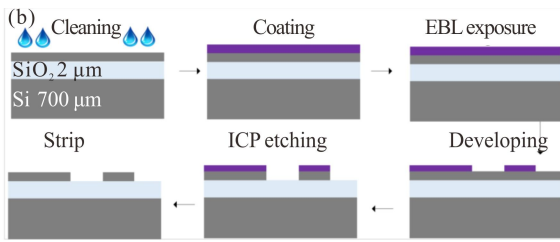


Fig.4 Device layout and process flow: (a) Positive layout of T-shaped waveguide coupled MRR and the vertical coupling grating; (b) Device processing flow

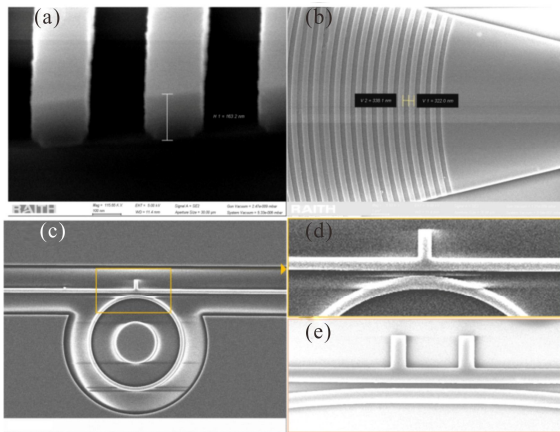


Fig.5 SEM images of silicon photonic devices: (a) Cross-section of vertical coupling grating; (b) Top view of vertical coupling grating; (c) T-shaped waveguide coupling MRR; (d) Single T-shaped waveguide; (e) Double-T-shaped waveguide

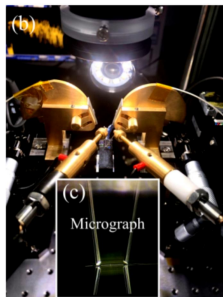
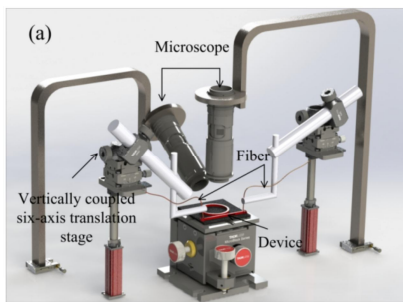
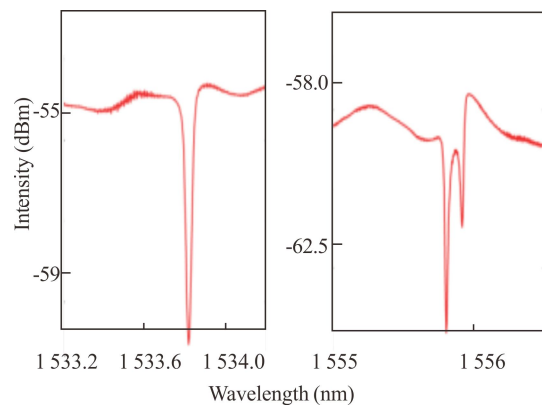
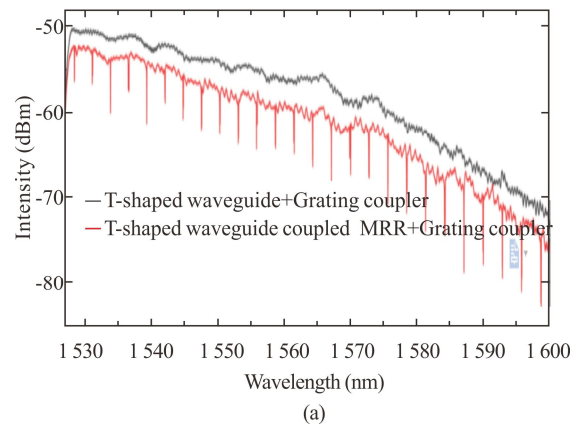


Fig.6 Device testing setup: (a) Semi-automatic chip coupling test platform; (b) Optical waveguide and vertical coupling grating's alignment area; (c) Microscopic alignment part collected from the rear coupling auxiliary lens

Fig.7 shows the transmission spectra of the single T-shaped waveguide coupled MRR with a wavelength ranging from 1 530 nm to 1 600 nm. We can see that every resonant peak presents a Fano resonance lineshape, and the full resonance peak has an antisymmetric lineshape. The free spectral range (*FSR*) is about 2.8 nm. The maximum *ER* of the Fano lineshape exceeds 10 dB, and the *SR* is 220.5 dB/nm (at 1 587.04 nm), both of which are smaller than the results calculated by FDTD (*SR* and *ER* are 265 dB/nm and 35 dB, respectively). The main reason is that the roughness of the processed edge is large, which makes the scattering loss prominent, which causes the *Q* value of the MRR resonant cavity to be slightly smaller. In addition, the coupling distance between the T waveguide and the MRR is 142 nm, and the coupling coefficient does not match the cavity loss. The partial enlargement of the spectrum in Fig.7(b) shows that the mode splitting occurs in the transmission mode. The symmetrical microring resonator mode is degenerate in theory. Clockwise (CW) and counter-clockwise (CCW) propagations exist simultaneously in the microring, and the modes do not degenerate. The surface roughness on the edge of the waveguide destroys the symmetry of propagation, and the CW and CCW modes no longer degenerate. If the line width of the resonance is small enough and the two modes can be distinguished, resonance splitting would occur in the output signal^[14].



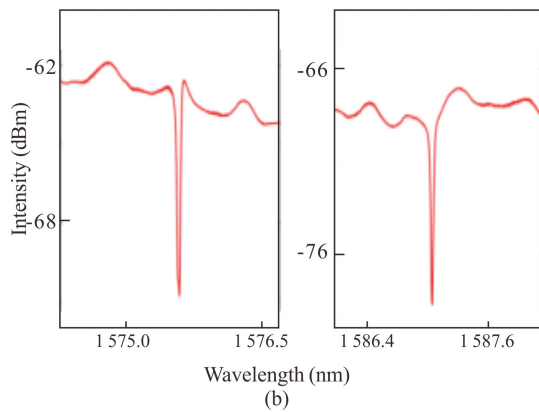


Fig.7 Single T-shaped waveguide coupled MRR's transmission spectra: (a) Transmission spectra of MRR (microring radius of 30 μm); (b) Details for several resonance peaks

By introducing the double-T-shaped waveguide into the bus waveguide to increase the phase factor value, the other parameters of the MRR remain unchanged, and the measured transmission spectra are shown in Fig.8(a). The transmission spectrum of the double-T-shaped waveguide coupled MRR shows a Fano resonance lineshape in every resonant peak, and its spectral period is determined by the *FSR* of the MRR ($FSR \approx 2.8 \text{ nm}$), which is close to the above FDTD calculation result. The maximum *ER* of the Fano line exceeds 15 dB, and the *SR* is 251.3 dB/nm (at 1574.1 nm), but both *SR* and *ER* are larger than those of the single T-shaped waveguide, and the phase factor introduced by the double-T-shaped waveguide is larger than that of the single T-shaped waveguide. The phase factor and coupling coefficient setting are closer to the best inflection point. As shown in Fig.8(b), the asymmetry of the Fano resonance lineshape at the long-wave resonance wavelength is more significant, which may be due to the difference in the phase factor and coupling coefficient from material dispersion. Due to the randomness of the machining process error, the transmission mode of the double-T-shaped waveguide coupled MRR device has mode splitting, which is improved compared with the single T-shaped waveguide coupled MRR. Similarly, the phase factor introduced by the double-T-shaped waveguide causes the mode to split the two modes, appearing as Fano resonance.

We designed a compact Fano resonant device, a T-shaped bus waveguide coupled MRR structure. All resonant mode lineshapes are asymmetric Fano resonance. The Fano lineshape produced by the T-shaped waveguide coupling MRR with different coupling gaps has high process tolerance in structural design and manufacturing. In the experiment, the maximum *ER* of the Fano lineshape exceeds 15 dB, and the *SR* is 251.3 dB/nm (at 1574.1 nm). The size of the Fano resonant device is equivalent to that of the MRR. The design of the device itself does not consider the influence of temperature. In practical applications, the influence of

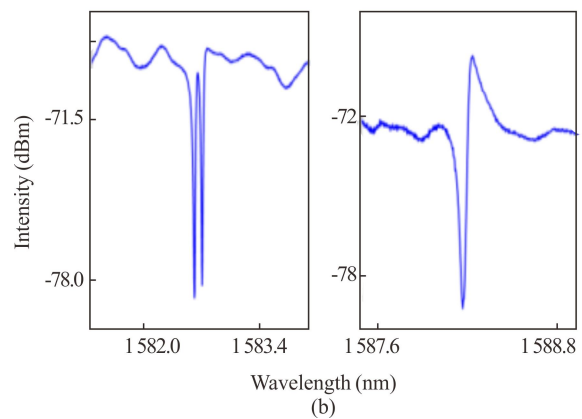
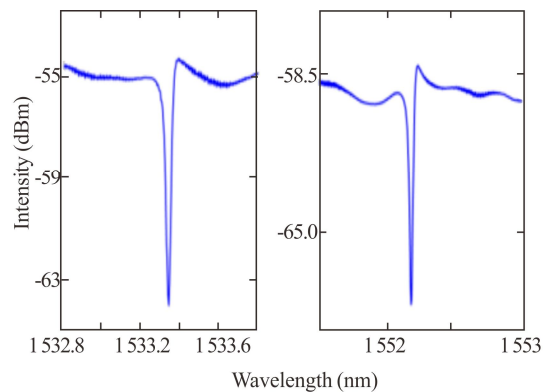
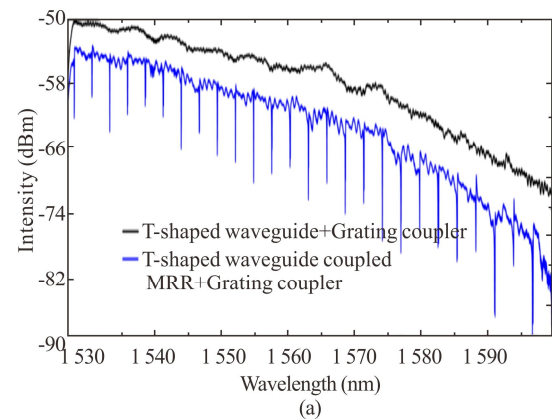


Fig.8 Double-T-shaped waveguide copled MRR's transmission spectra: (a) Transmission spectra of MRR (microring radius of 30 μm); (b) Details for several resonance peaks

temperature changes on the sensor should be effectively avoided.

Statements and Declarations

The authors declare no conflicts of interest related to this article.

References

[1] FANO U. Effects of configuration interaction on intensities and phase shifts[J]. Physical review, 1961, 124(6): 1866.

- [2] LIDE D R. A century of excellence in measurements, standards, and technology[M]. Boston: Government Printing Office, 2017: 116-119.
- [3] ZHAO C Y, ZHANG L, ZHANG C M. Compact SOI optimized slot microring coupled phase-shifted Bragg grating resonator for sensing[J]. Optics communications, 2018, 414: 212-216.
- [4] ZHOU X, ZHANG L, ARMANI A M, et al. On-chip biological and chemical sensing with reversed Fano lineshape enabled by embedded microring resonators[J]. IEEE journal of selected topics in quantum electronics, 2013, 20(3): 35-44.
- [5] PENG F, WANG Z, YUAN G, et al. High-sensitivity refractive index sensing based on Fano resonances in a photonic crystal cavity-coupled microring resonator[J]. IEEE photonics journal, 2018, 10(2): 1-8.
- [6] ZHANG J, LEROUX X, DURÁN-VALDEIGLESIAS E, et al. Generating Fano resonances in a single-waveguide silicon nanobeam cavity for efficient electro-optical modulation[J]. ACS photonics, 2018, 5(11): 4229-4237.
- [7] CHEN S, ZHOU G, ZHOU L, et al. High-linearity Fano resonance modulator using a microring-assisted Mach-Zehnder structure[J]. Journal of lightwave technology, 2020, 38(13): 3395-3403.
- [8] MENG Z M, CHEN C B, QIN F. Theoretical investigation of integratable photonic crystal nanobeam all-optical switching with ultrafast response and ultralow switching energy[J]. Journal of physics D: applied physics, 2020, 53(20): 205105.
- [9] YU Y, HEUCK M, HU H, et al. Fano resonance control in a photonic crystal structure and its application to ultrafast switching[J]. Applied physics letters, 2014, 105(6): 061117.
- [10] ZHENG S, CAO X, WANG J. Multimode Fano resonances for low-power mode switching[J]. Optics letters, 2020, 45(4): 1035-1038.
- [11] LU Y, XU L, YU Y, et al. Double-wavelength Fano resonance and enhanced coupled-resonator-induced transparency in a double-microcavity resonator system[J]. Journal of the optical society of America A, 2006, 23(7): 1718-1721.
- [12] GU L, FANG L, FANG H, et al. Fano resonance lineshapes in a waveguide-microring structure enabled by an air-hole[J]. APL photonics, 2020, 5(1): 016108.
- [13] LU L, ZHU L, ZENG Z, et al. Fano resonance ion sensor enabled by 2D plasmonic sub-nanopores-material[J]. IEEE sensors journal, 2021, 21(13): 14776-14783.
- [14] WERQUIN S. Optimizations of a ring resonator biosensor platform for applications in DNA detection[D]. Ghent: Ghent University, 2015.